NUCLEAR SCIENCE AND TECHNIQUES **26**, 010101 (2015)

Developments at SSRF in soft X-ray interference lithography*

YANG Shu-Min (杨树敏),[1] WANG Lian-Sheng (王连升),[1] ZHAO Jun (赵俊),[1] XUE Chao-Fan (薛超凡),[1]
LIU Hai-Gang (刘海岗),[1] XU Zi-Jian (许子建),[1] WU Yan-Qing (吴衍青),[1,†] and TAI Ren-Zhong (邰仁忠)[1,‡]

[1]*Shanghai Institute of Applied Physics, Chinese Academy of Sciences, Shanghai Synchrotron Radiation Facility, Shanghai 201800, China*

(Received September 17, 2014; accepted in revised form November 14, 2014; published online February 2, 2015)

The soft X-ray interference lithography (XIL) branch beamline at Shanghai Synchrotron Radiation Facility (SSRF) is briefly introduced in this article. It is designed for obtaining 1D (line/space) and 2D (dot/hole) periodic nanostructures by using two or more coherent extreme ultraviolet (EUV) beams from an undulator source. A transmission-diffraction-grating type of interferometer is used at the end station. Initial results reveal high performance of the beamline, with 50 nm half-pitch 1D and 2D patterns from a single exposure area of 400 μm × 400 μm. XIL is used in a growing number of areas, such as EUV resist test, surface enhanced Raman scattering (SERS) and color filter plasmonic devices. By using highly coherent EUV beam, broadband coherent diffractive imaging can be performed on the XIL beamline. Well reconstructed pinhole of ϕ20 μm has been realized.

Keywords: Extreme ultraviolet, Soft x-ray interference lithography, Periodic nanostructures, Grating, Half-pitch

DOI: 10.13538/j.1001-8042/nst.26.010101

I. INTRODUCTION

Large area high resolution periodic nanostructures are needed in many areas of scientific research, such as gratings for spectroscopy, bio-sensor arrays, surface plasmon, photonic crystals and magnetic recording. Lithography methods of electron beam lithography (EBL), nanoimprint lithography (NIL), scanning probe lithography (SPL) and laser interference lithography (LIL) can be used to prepare periodic nanostructures [1–4]. EBL and SPL are of high resolution, but they are too slow to obtain large area nanostructures. NIL costs less, but has problems of particulate contamination and residual polymer layer [5] on the nanostructures. LIL can also be used to print periodic nanostructures over large area, with low cost, too, but the resolution is limited to 100 nm by wavelength of laser [6].

Based on coherent radiation from undulator source, soft X-ray interference lithography (XIL) is developed for preparing large area periodic nanostructures in resolutions below 100 nm [7]. Modern synchrotrons can provide highly coherent radiations up to about 100 eV [8]. XIL beamlines have been built in different synchrotron facilities, such as the XIL II beamline in SLS [9], the EUV-IL beamline in NewSUBARU [10], the EUV-IL beamline in Wisconsin-Madison [11], the EUV-IL beamline in the NSRRC (Taiwan) [12], and the highest resolution, lines structures below 8 nm, is obtained by XIL techniques up to now [9].

In this paper, we report the latest developments and potential applications of XIL branch beamline (BL08U1B) at Shanghai Synchrotron Radiation Facility (SSRF). Based on diffraction (gratings) optics, 50 nm half-pitch 1D and 2D periodic patterns with single exposure area of 400 μm × 400 μm were obtained. Also, broadband coherent diffractive imaging was carried out on the XIL experimental setup, with good results.

II. BEAMLINE LAYOUT

The XIL beamline is a branch of the soft X-ray spectromicroscopy beamline (STXM, BL08U1A) [13] using the elliptically polarized undulator (EPU). Energy range of the XIL is 85–150 eV. According to the choice of next-generation EUV lithography technology, the EPU gap is usually set at 37.47 mm, corresponding to energy of 92.5 eV [14]. The beamline layout is shown in Fig. 1. A four-knife slit (Slit1) located at 20 m from the source point is employed to define the acceptance angles to ±0.04 mrad in horizontal and vertical directions. Slit 1 also functions to absorb most of the heat load and protect the downstream optical elements. After Slit 1, two cylinder mirrors, Au-coated and side water-cooled, are used to deflect and focus the beam. The beam is diverted into the XIL branch when the Mirror 1 is inserted into the main beam. It deflects the beam horizontally by 1.5° and produces light parallel in the vertical direction. It plays a role in cutting the higher energy radiation (> 2000 eV). The Mirror 2 deflects the beam by 10°, which is large enough to eliminate photons in energies of above 150 eV. It plays a role in cutting higher harmonic, and it deflects and focuses the beam to another four-knife slit (Slit2), which acts as the high quality spatial coherence second light source for the transmission-diffraction-grating at the end station. The measurement results in acceptance of the beamline are shown in Table 1.

The XIL chamber, with an interferometer (mask) of the transmission-diffraction-grating type [15, 16], is installed in a 100-class clean room at the end of the beamline. The spatially

* Supported by the National Key Basic Research Program of China (No. 2012CB825700) and the Open Research Project of Large Scientific Facility from Chinese Academy of Sciences: Study on Self-Assembly Technology and Nanometer Array with Ultra-high Density

† Corresponding author, wuyanqing@sinap.ac.cn

‡ Corresponding author, tairenzhong@sinap.ac.cn

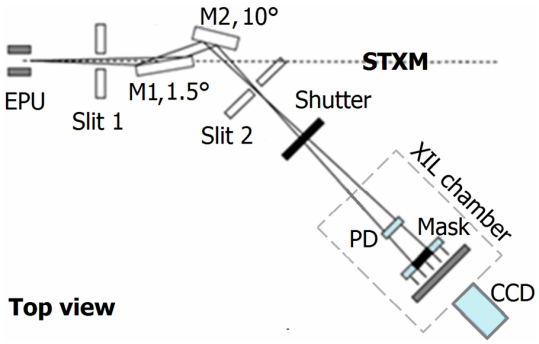

Fig. 1. (Color online) Schematic layout of the BL08U1B beamline.

TABLE 1. Measurement results of the BL08U1B beamline in its acceptance test

Items	Measurement results
Photon energy (eV)	85–150
Spot size at mask (mm)	3.1×3.1@85 eV
	3.1×3.1@92 eV
	3.1×3.1@150 eV
Flux at mask (10^{15} s^{-1} cm^{-2})	2.4@85 eV
	3.6@92 eV
	0.93@ 150 eV
Single exposure size (mm)	0.4×0.4
Fringe period (nm)	100

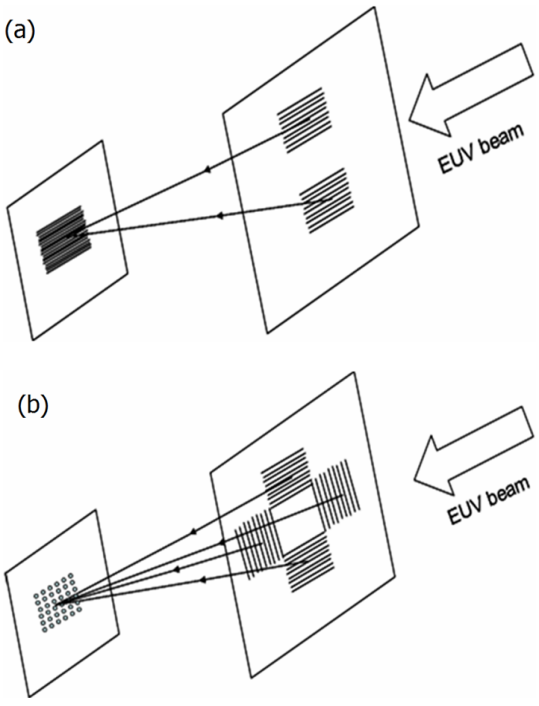

Fig. 2. (Color online) The schemes of grating based interference. 1D line patterns and 2D dot patterns will be fabricated respectively.

coherent incident beam is diffracted by linear gratings which are patterned on a Si_3N_4 membrane (Fig. 2). The resulting mutually coherent beams interfere at a certain distance along

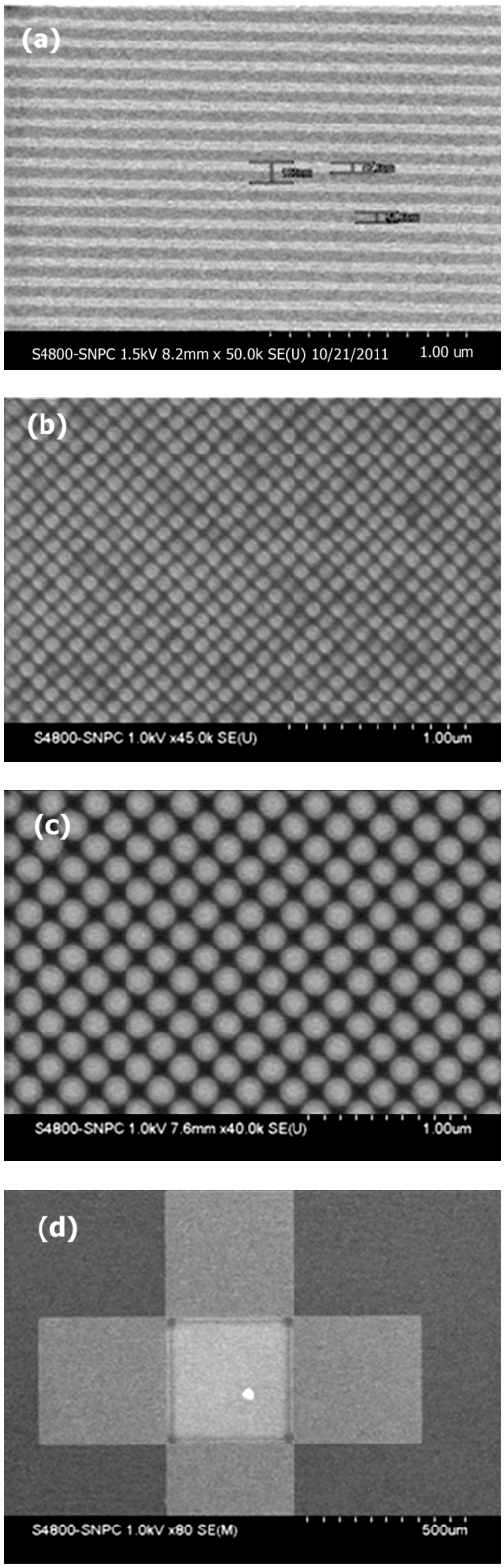

Fig. 3. Periodic line and hole patterns made by XIL exposure in PMMA using different masks. (a) 50 nm half-pitch lines, (b, c) 50 and 100 nm half-pitch holes, (d) SEM image of the single exposure area of 400 microns. The scanning mode is SEM (U).

the beam direction. The exposure dose is detected by a photodiode (PD) installed before the mask. Two linear gratings are used to create lines (Fig. 2(a)), while hole/dot patterns can be made in one exposure step by the interference of three or more diffracted beams (Fig. 2(b)).

For two-beam interference, considering normal incidence of the light, pitch size of the interference fringes is expressed as $p = d/2$, where d is pitch size of the grating pattern. For multi-beam interference, the relationship between the period of diffraction gratings and the fringe patterns varies depending on the grating design [16, 17]. For example, in a four-beam scheme, a demagnification factor of 2 or $2^{1/2}$ (in terms of pattern period) can be obtained when the phases factor difference of the interfering beams are $n\pi$ or $(n + 1/2)\pi$, where n is an integer [17]. Thus, the period of the fringe pattern is related to the grating period only and is independent of the illuminating wavelength (Fig. 2). Thus, high power of broadband radiation from the undulator sources can be used efficiently. A larger spectral width of the illuminating source is permitted to have a higher illuminating flux. Then the exposure time can be shortened, and the vibration issues can be avoided as much as possible. Spectral width of the beamline is 1/40, which leads to high flux (Table 1). Under such high flux, hole and line patterns in polymethyl methacrylate (PMMA) resist can be exposed within 30 s on the beamline.

Examples of line and holes patterns of various periods, which were realized on the XIL beamline, are shown in Fig. 3. Structures of 1D periodic lines structures, and 2D periodic holes with the half-pitch of 50 nm, and 100 nm, are shown in Figs. 3(a), 3(b) and 3(c), respectively. Fig. 3(d) is SEM image of the single exposure area, sized at 400 μm. Depending on the grating structures, the exposure time was 10–30 s, which is much quicker than traditional EBL techniques. All the above structures were exposed in positive PMMA resist, in thickness of 70 nm, spin-coated on Si wafers. After exposure, the samples were developed in 1:3 solution of methyl isobutyl ketone (MIBK): isopropyl alcohol (IPA) for 30 s.

The exposure structures in Fig. 3 look like dot array not hole array. This is very strange. As positive resist, the exposed PMMA can be removed after developing by MIBK: IPA and 2D hole arrays should be obtained. This may be because of non-conductive of the resist and the scanning mode in the SEM. SEM (U) mode is usually used to get a clear image (Fig. 3) because of the non-conductive resist. Pictures of hole arrays can be obtained when the SEM (L) mode is used (Fig. 4(a)). But it is not so clear. In addition, hole arrays can be clearly seen in the AFM image (Fig. 4(b)). The above SEM pictures were monitored by field-emission scanning electron microscopy (FE-SEM, Hitachi S-4800). The gratings were bought from Eulitha AG.

III. TRANSMISSION GRATING FABRICATION

Grating is a key part of XIL techniques [16–20]. We had to buy gratings from Eulitha AG before we bought the EBL machine (Crestec Cabl-9500C) in 2013, since then two-beam grating in 300-nm period has been made and used.

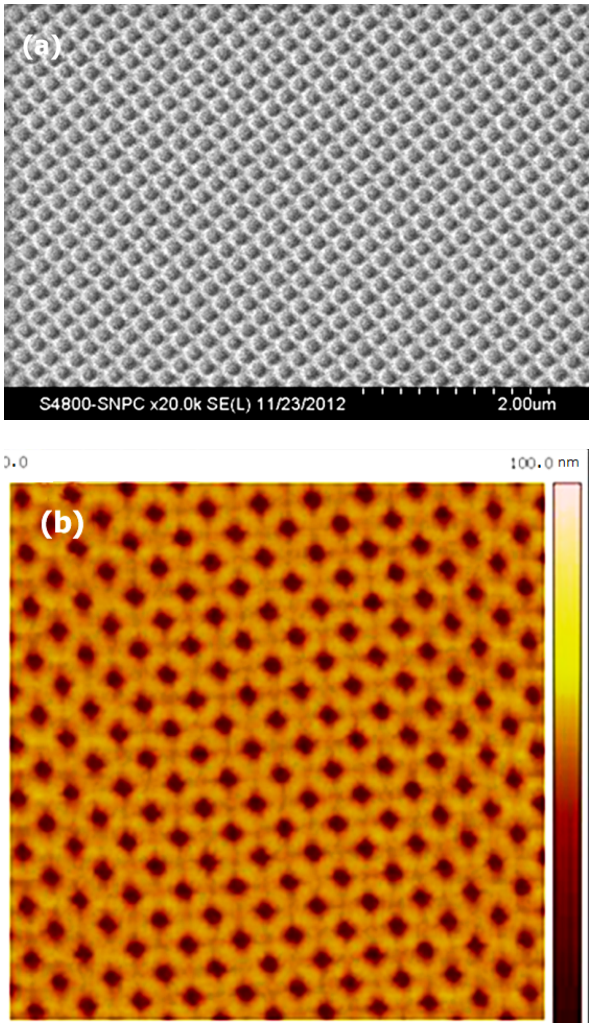

Fig. 4. (Color online) SE (L) image (a) and AFM image (b) of 100 nm half-pitch periodic hole patterns.

Dry-etching and lift-off process are usually used in the grating fabrication process [16–18]. Smooth and steep Cr line structure can be fabricated by using the dry-etching process. However, poisonous gas such as Cl_2 is usually used in the etching process. Zhu *et al*. [19, 20] reported that by means of electron beam evaporation and lift-off process, smooth Cr line structure was fabricated. Based on the rigorous coupled-wave analysis, they fabricated a Cr grating on 100 nm Si_3N_4 membrane by using the EBL lithography and the lift-off process. The first order diffraction efficiency of the grating is 4.43%. By using the same process, we obtained a Cr grating with period of 300 nm and obtained its exposure results in XIL beamline.

The grating fabrication process is schematically shown in Fig. 5(a). A low-stress 100 nm Si_3N_4 layer was chosen as the transparent membrane. A Crestec CABL-9500C e-beam lithography tool was used for the lithography. After lithography, a 50 nm Cr layer was deposited by electronic beam evaporation. A 300 nm thick Au was deposited onto the outside grating region by electronic beam evaporation. It acted

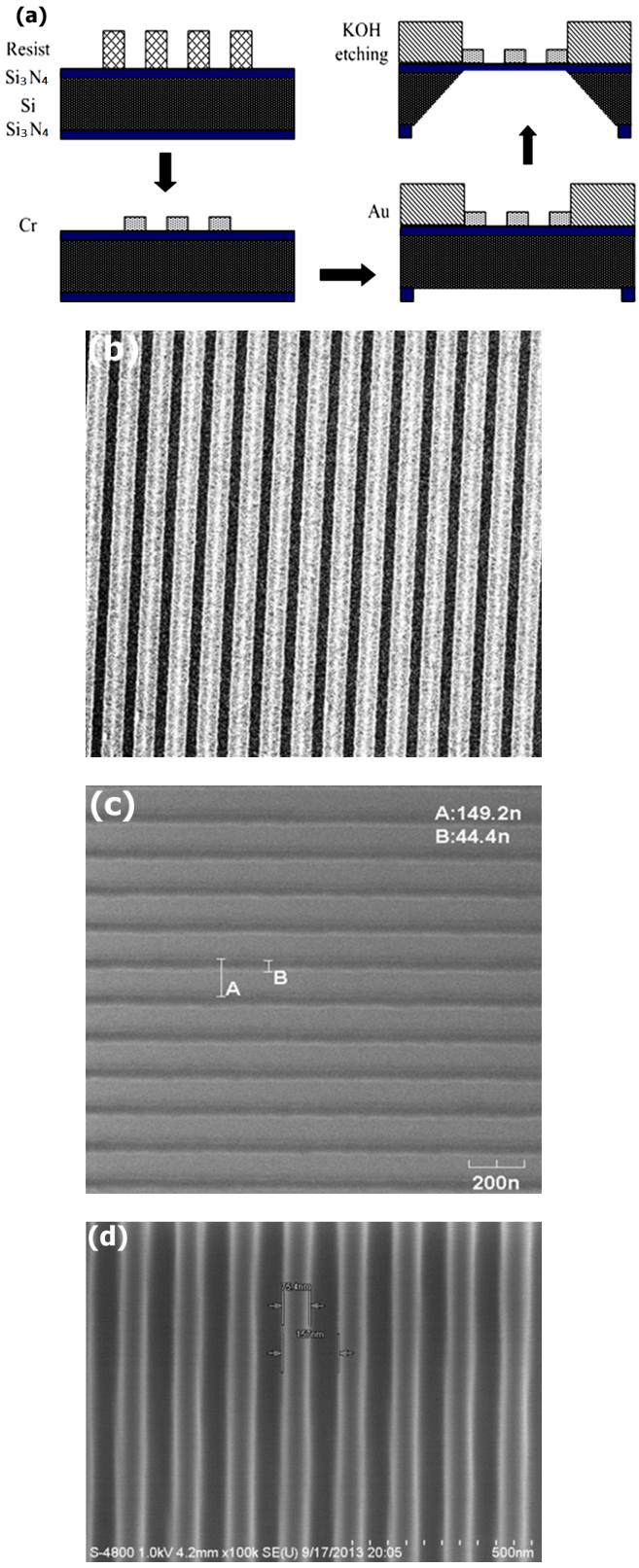

Fig. 5. (Color online) Fabrication process of the gating (a), SEM image of the two beam grating (b), and SEM image of the exposure result on PMMA (c), and on the user's MG resist (d).

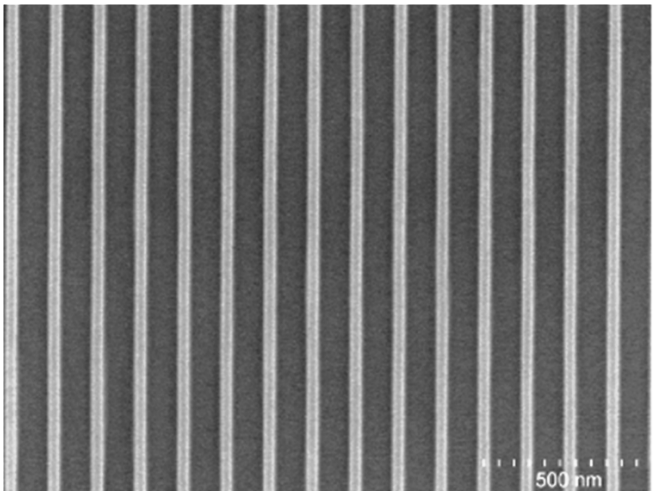

Fig. 6. SEM image of the XIL patterns on MG resist invented by Yang *et al*. [21].

as an XIL grating central photon stop layer. The backside silicon substrate was removed by a wet-etch process using an aqueous KOH solution at 80 °C. Fig. 5(b), Fig. 5(c) and Fig. 5(d) show SEM images of the Cr grating and its interference patterns (half-pitch=75 nm) on PMMA resist and on a molecular glass (MG) resist invented by one of users. SEM imaging of the grating and the exposure result on PMMA were monitored by SEM function of the EBL system (CABL-9500C), and SEM imaging of the exposure result done by our user was monitored by field-emission scanning electron microscopy (FE-SEM, Hitachi S-4800).

IV. APPLICATIONS

The XIL beamline, started commissioning in Sept. 2011 and operation in Jan. 2012, has been opened to users since Oct. 2012. Thanks to its excellent performance in terms of pattern resolution, uniformity, size of the pattern area, the system has been used in numerous applications, such as EUV resist test, surface-enhanced Raman scattering, nanometer magnetism, biology self-assembly, nano-photoelectron device, and large area gratings of high density. Up to now, 10 patents and 7 articles have been published. Here we report the applications in EUV resist test and surface enhanced Raman scattering.

A. EUV resist test with high resolution [21]

EUV lithography with 13.4 nm irradiation is most likely to be used for the next-generation lithography. It is a key technology for continuation of the Moor's Law [22]. Challenges in EUV lithography include the EUV lithography system, mask, and photoresist [23]. Yang *et al.* [21] did EUV resist test on the soft XIL beamline. By changing the exposure time, they obtained line structures of different line width on

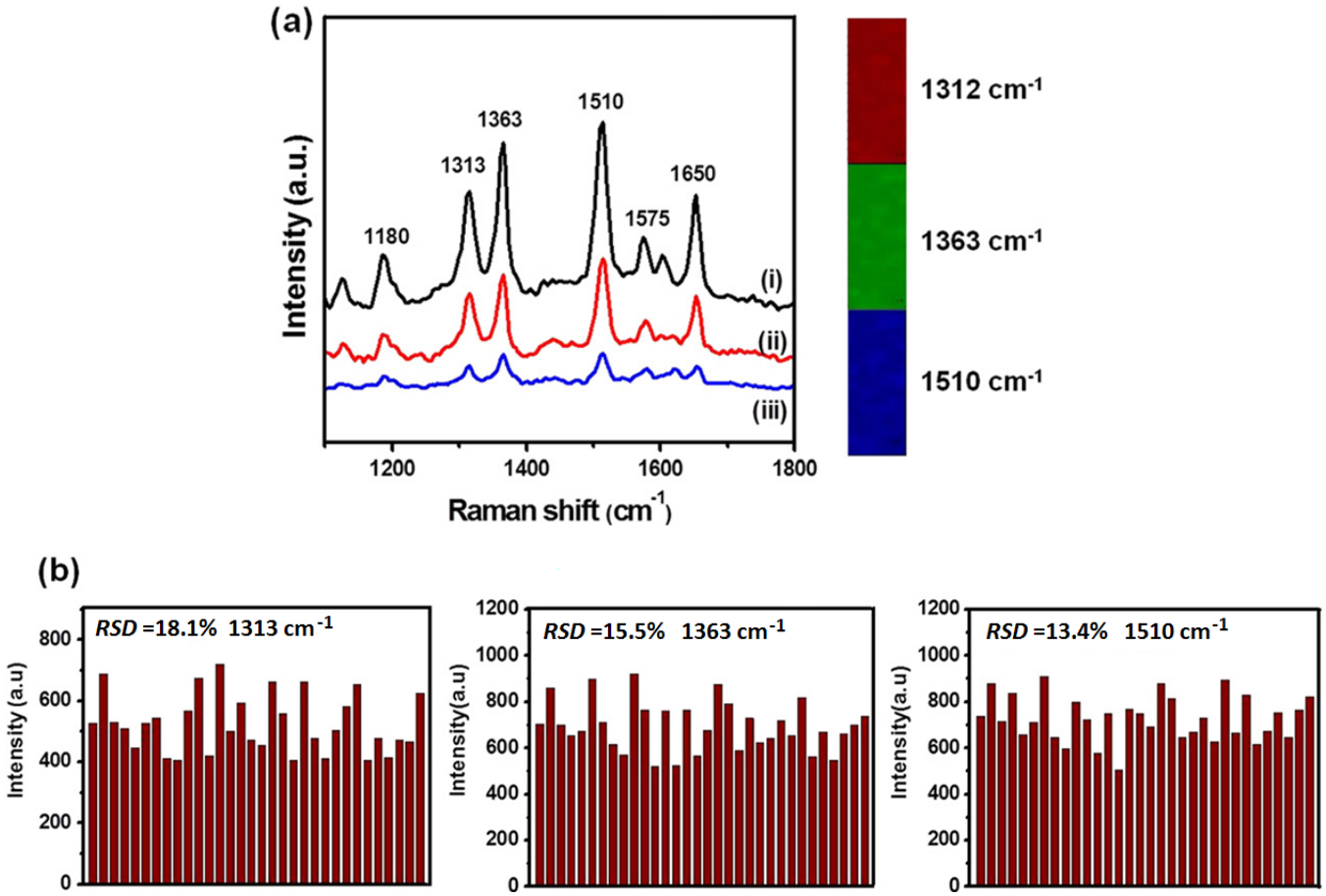

Fig. 7. (Color online) Surface enhanced Raman scattering of R6G on the Au nanodisk array with high resolution and high uniformity [24].

the MG resist they invented. Line structure in 30 nm resolution and line width roughness (LWR) of 2 nm was obtained (Fig. 6).

B. Surface enhanced Raman scattering (SERS) with high sensitivity and uniformity [24]

Au nanodisk arrays exhibited a significant, uniform and reproducible surface enhancement on Raman scattering signal, which enabled the detection of R6G (Rhodamine 6G) as low as 10^{-8} M with an enhancement factor of 10^6 (Fig. 7(a)). Importantly, the Au nanodisk arrays SERS-active substrates with uniform high sensitivity have high reproducibility and stability. Intensities of the main Raman vibrations of R6G methanol solution in 32 spot SERS spectra were collected on the Au nanodisk arrays. The values of RSD (relative standard deviation) of vibrations at 1313, 1366 and 1512 cm^{-1} are 18.1%, 15.5%, and 13.4% (Fig. 7(b)), respectively, which a vigorous indication of the substrate uniformity [24]. XIL nanofabrication appears to be a feasible approach to prepare uniform and reproducible SERS-active substrates with high sensitivity for practical SERS applications.

V. LATEST DEVELOPMENT-BROADBAND COHERENT DIFFRACTIVE IMAGING

Broadband coherent diffractive imaging (CDI) is the latest development on the XIL beamline. CDI is a powerful microscopy technique for imaging materials and biological specimens in two and three dimensions [25]. It does not rely on X-ray optics, so its spatial resolution is just limited by the wavelength. Significant increases in the spatial resolution require brighter sources and longer exposure time, or the capacity of increasing the acceptable limit on the bandwidth. The use of broadband X-ray beams is a possible way to improve the spatial resolution [26].

Using full spectrum width of the undulator radiation enables a broadband XIL lithography. The beam spatial coherence and coherent photon flux can be controlled precisely, which meets the conditions of broadband coherent diffractive imaging. Then, broadband CDI can be carried out on the XIL beamline. Typical results are shown in Fig. 8. Broadband X-rays, in a distribution shown in Fig. 8(a), and in normal incidence, irradiated on a ϕ20 μm pinhole. Fig. 8(b) shows the diffraction pattern collected by CCD. Fig. 8(c) shows the pinhole image reconstructed after enough iteration by broadband phase retrieval algorithm. Comparing with Fig. 8(d),

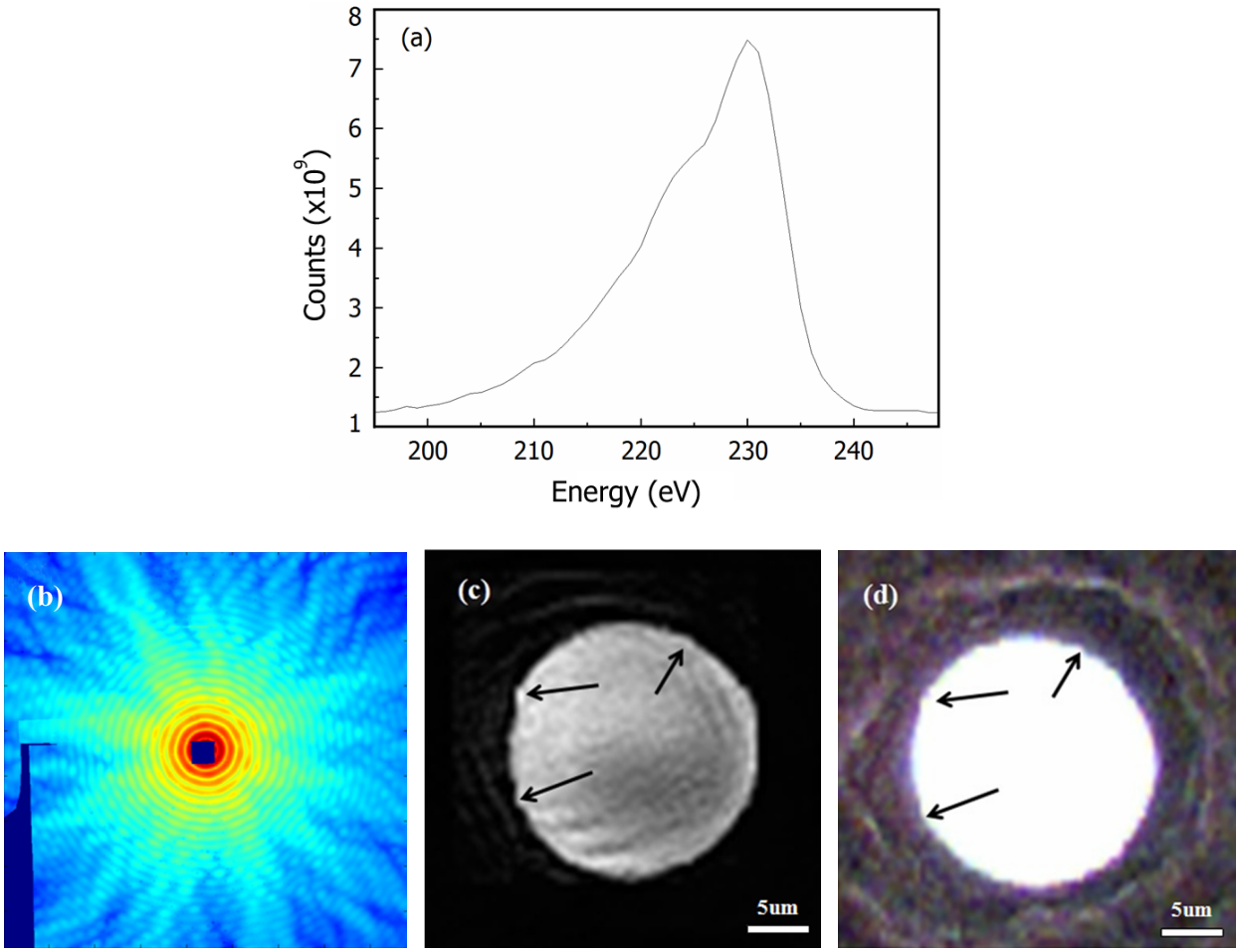

Fig. 8. (Color online) Typical results of broadband CDI. (a) First harmonic spectrum of undulator radiation. (b) Diffraction pattern of pinhole (in logarithmic scale), the central and left show missing signals caused by the beamstop. (c) Reconstructed pinhole image. (d) The pinhole STXM image.

we can see that the reconstructed pinhole image is the same as its real image, and the aperture edge detail is clearly visible (shown the arrow positions). In order to avoid saturating the CCD, a beamstop is used, which causes black fake signals appearing inside the reconstructed pinhole image because of the central missing signal in Fig. 8(b). The central missing data can be estimated by Fourier transform of lower resolution images by, e.g., soft X-ray microscopes [27]. The results demonstrate the application of broadband CDI in XIL, which provides a prerequisite for developing rapid high-resolution three dimensional imaging technique.

VI. CONCLUSION

In this study, a new branch beamline in SSRF to perform XIL exposure is introduced. A transmission-diffraction type of grating is used on the beamline. The XIL beamline can be used to fabricate 1D periodic line structures and 2D periodic holes patterns by using the EUV exposure of two- or multi-beam gratings. A two-beam Cr transmission diffraction grating of 300 nm pitch was fabricated by the lift-off process. High quality exposure line patterns with the half-pitch of 75 nm were fabricated on PMMA and MG resist. EUV resist test with high resolution and surface enhanced Raman scattering detection with high sensitivity and uniformity have been realized by the beamline users. These show excellent performance of the XIL beamline. By using the highly coherent EUV beam, XIL beamline can be used to perform broadband CDI. Well reconstructed pinhole of ϕ20 μm has been realized on the beamline.

[1] Tavakkoli A, Piramanayagam S N, Ranjbar M, *et al*. Path to achieve sub-10-nm half-pitch using electron beam lithography. J Vac Sci Technol B, 2011, **29**: 011035. DOI: 10.1116/1.3532938

[2] Guo L J. Nanoimprint lithography: Methods and material requirements. Adv Mater, 2007, **19**: 495–513. DOI: 10.1002/adma.200600882

[3] Sidorkin V, Veldhoven E, Drift E, *et al*. Sub-10-nm nanolithography with a scanning helium beam. J Vac Sci Technol B, 2009, **27**: L18-20. DOI: 10.1116/1.3182742

[4] Brueck S R J. Optical and interferometric lithography - nanotechnology enablers. Proc IEEE, 2005, **93**:1704–1721. DOI: 10.1109/JPROC.2005.853538

[5] Xie C Q, Zhu X. L, Niu J B, *et al*. Micro- and nanometal structures fabrication technology and applications. Acta Opt Sinica, 2011, **31**: 0900128. (in Chinese) DOI: 10.3788/AOS201131.0900128

[6] Savas T A, Schattenburg M L, Carter J M, *et al*. Large-area achromatic interferometric lithography for 100 nm period gratings and grids. J Vac Sci Technol B, 1996, **14**: 4167–4170. DOI: 10.1116/1.588613

[7] Solak H H. Nanolithography with coherent extreme ultraviolet light. J Phys D, 2006, **39**: R171. DOI: 10.1088/0022-3727/39/10/R01

[8] Attwood D, Halbach K and Kim K J. Tunable coherent X-rays. Science, 1985, **228**: 1265. DOI: 10.1126/science.228.4705.1265

[9] Ekinci Y, Vockenhuber M, Hojeij M, *et al*. Evaluation of EUV resist performance with interference lithography towards 11 nm half-pitch and beyond. Proc SPIE, 2013, **8679**: 867910-11. DOI: 10.1117/12.2011533

[10] Shiotani H, Suzuki S, Lee D G, *et al*. Dual grating interferometric lithography for 22-nm node. Jpn J Appl Phys, 2008, **47**: 4881–4885. DOI: 10.1143/JJAP.47.4881

[11] Isoyan A, Wüest A, Wallace J, *et al*. 4X reduction extreme ultraviolet interferometric lithography. Opt Express, 2008, **16**: 9106–9111. DOI: 10.1364/OE.16.009106

[12] Lin C H, Fong C H, Lin Y M, *et al*. EUV interferometric lithography and structural characterization of an EUV diffraction grating with nondestructive spectroscopic ellipsometry. Microelectron Eng, 2011, **88**: 2639–2643. DOI: 10.1016/j.mee.2011.02.002

[13] Xue C F, Wang Y, Guo Z, *et al*. High-performance soft x-ray spectromicroscopy beamline at SSRF. Rev Sci Instrum, 2010, **81**: 103502–103505. DOI: 10.1063/1.3491837

[14] W B Q and Ajay K. Extreme ultraviolet lithography: A review. J Vac Sci Technol B, 2007, **25**: 1743–1761. DOI: 10.1116/1.2794048

[15] Solak H H, David C, Gobrecht J, *et al*. Sub-50 nm period patterns with EUV interference lithography. Microelectron Eng, 2003, **67–68**: 56–62. DOI: 10.1016/S0167-9317(03)00059-5

[16] Solak H H. Space-invariant multiple-beam achromatic EUV interference lithography. Microelectron Eng, 2005, **78-79**: 410–416. DOI: 10.1016/j.mee.2005.01.012

[17] Solak H H, David C, Gobrecht J, *et al*. Multiple-beam interference lithography with electron beam written gratings. J Vac Sci Technol B, 2002, **20**: 2844–2848. DOI: 10.1116/1.1518015

[18] Fukushima Y, Sakagami N, Kimura T, *et al*. Development of extreme ultraviolet interference lithography system. Jpn J Appl Phys, 2010, **49**: 06GD06. DOI: 10.1143/JJAP.49.06GD06

[19] Zhu W Z, Wu Y Q, Chen M, *et al*. Optimized design of transmission grating used for 13.4 nm soft X-ray interference lithography. Acta Opt Sinica, 2008, **28**: 1225–1230. (in Chinese) DOI: 10.3788/AOS20082807.1225

[20] Zhu W Z, Wu Y Q, Guo Z, *et al*. The design, fabrication and performance of a large area 10000 line/mm metal transmission diffraction gratingsfor soft X-ray. Acta Phys Sinica, 2008, **57**: 6386–6392. (in Chinese) DOI: 10.7498/aps.57.6386

[21] Chen L, Xu J, Yuan H, *et al*. Outgassing analysis of molecular glass photoresists under EUV irradiation. Sci China Chem, 2014, **57**: 1746–1750. DOI: 10.1007/s11426-014-5122-y

[22] O'Sullivan G, Kilbane D, D'Arcy R. Recent progress in source development for extreme UV lithography. J Mod Opt, 2012, **59**: 855–872. DOI: 10.1080/09500340.2012.678399

[23] Kinoshita H, Watanabe T, Harada T, *et al*. Recent Activities on Extreme Ultraviolet Lithography in NewSUBARU. Jpn J Appl Phys, 2013, **52**: 06GA01. DOI: 10.7567/JJAP.52.06GA01

[24] Zhang P P, Yang S M, Wang L S, *et al*. Large-scale uniform Au nanodisk arrays fabricated via x-ray interference lithography for reproducible and sensitive SERS substrate. Nanotechnology, 2014, **25**: 245301. DOI: 10.1088/0957-4484/25/24/245301

[25] Chapman H N, Nugent K A. Coherent lensless X-ray imaging. Nat Photonics, 2010, **4**: 833–839. DOI: 10.1038/nphoton.2010.240

[26] Abbey B, Whitehead L W, Quiney H M, *et al*. Lensless imaging using broadband X-ray sources. Nat Photonics, 2011, **5**: 420–424. DOI: 10.1038/nphoton.2011.125

[27] Kirz J, Jacobsen C and Howells M. Soft X-ray microscopes and their biological applications. Q Rev Biophys, 1995, **28**: 33–130. DOI: 10.1017/S0033583500003139